International Journal of General Medicine

Dovepress

open access to scientific and medical research

Open Access Full Text Article

ORIGINAL RESEARCH

Mapping the Spatial Evolution of Proximal Femur Osteoporosis: A Retrospective Cross-Sectional Study Based on CT Scans

Robert B Bot[1,2], Razvan Chirla[1], Calin Tudor Hozan[1,2], Simona Cavalu[1]

[1]Faculty of Medicine and Pharmacy, University of Oradea, Oradea, 410087, Romania; [2]Department of Orthopedics, Emergency County Clinical Hospital Oradea, Oradea, 410169, Romania

Correspondence: Simona Cavalu, Email scavalu@uoradea.ro

Purpose: The purpose of this study was to quantify the modifications occurring in osteoporosis at the level of the human proximal femur throughout the trabecular structure, along with the identification of certain anatomic regions preferentially affected by osteoporosis. Another goal was to map the evolution of the radiodensity of the trabecular bone as osteoporosis progresses to an advanced stage.

Methods: The study included CT scans (right femur) from 51 patients, out of which 40 had various degrees of osteoporosis, but no other local pathology. Ten regions of interest in two orthogonal slices have been identified and the differences in radiodensity as well as their evolution have been statistically analyzed in terms of relative and absolute changes.

Results: A detailed spatial map showing the evolution of osteoporosis was obtained. As osteoporosis evolved, the relative decrease in radiodensity was inversely correlated to the radiodensity of the healthy bone. In particular, the region covering the Ward triangle decreased the most, by an average 61–62% in osteopenia and 101–106% in advanced osteoporosis, while the principal compressive group was affected the least, showing a decrease by an average 14–15% in osteopenia and 29–32% in advanced osteoporosis. The absolute decrease in radiodensity was not correlated to the radiodensity of the healthy bone and was shifted to the inferior-posterior edge of the femur. Inside the femoral head, the upper region was affected the most in absolute terms, while the greater trochanter was less affected than the femoral neck. The maximum metaphyseal cortical bone density was unaffected by the progression of osteoporosis.

Conclusion: Significant differences were noticed in terms of the absolute and relative osteoporotic changes in radiodensity related to different anatomical regions of the human femoral bone. These differences become more pronounced as the disease progresses.

Keywords: osteoporosis, radiodensity, CT, femur

Introduction

Femoral neck fractures represent a global public health issue due to their high incidence and the impact on the patient's quality of life and on the health care system, involving significant costs.[1] In 2019, approximately 290,000 patients with hip fractures were hospitalized just in the USA.[2] Over 90% of hip fractures are caused by falls,[3] and 60% of them are intracapsular.[4] They affect mostly the elderly, being a consequence of low energy falls, while in young patients, hip fractures mainly occur due to high energy traumas (eg, road accidents, sports injuries and falls from large heights).[5] Predicting human proximal femur fractures is a very difficult task, involving details of bone mechanical properties, complex bone geometry and boundary conditions as well. Different finite element models of crack propagation and fracture models were developed in order to predict the onset of human femoral neck fracture under excessive load, but these computational simulation techniques need to be validated by more extensive ex-vivo experiments.[6–8] It is generally accepted that osteoporosis patients have a higher risk of major fracture.[9] The prevalence of osteoporosis and osteopenia in the aging population is significantly higher in women than men, with significant differences between various countries and races.[10] Different patterns of focal osteoporosis were observed in femoral neck and trochanteric fracture patients,

Received: 11 January 2024
Accepted: 12 March 2024
Published: 21 March 2024

showing the preferential locations in the proximal femur where cracks are expected to initiate during falls. Moreover, the same anatomical areas are at risk of rapid bone loss with ageing.[11]

It is well known that bone demineralization occurs with age. Numerous authors have studied the trabecular system of the proximal femur and the changes that occur at this level with ageing, by using clinical CT, MicroCT, pQCT, as well as dual X-ray absorptiometry (DXA),[12–17] confirming more pronounced modifications in elderly women.[18–21] DXA is the gold standard when it comes to clinical bone density measurement, while another useful method for assessing bone density in the proximal femur is based on radiological examination and the assessment of the Singh index.[22–24] Employing deep learning techniques[25] and applying various filters can improve the accuracy of the results.[26] MRI can provide precise information, but is challenging to implement as a routine investigation for assessing bone density.[27,28]

For more effective prevention and better predictability of femoral neck fractures, as well as to achieve improved postoperative outcomes, it is essential to understand bone behavior at the level of the proximal femur, particularly the trabecular system, as it transforms with age and throughout the evolution of osteoporosis. Understanding the anatomical locations of the weak areas in the neck and head of the femur, as well as the locations of the regions with increased bone density, enables the determination of the optimal path for the osteosynthesis material employed to fix femoral neck fractures, ensuring it passes through the regions with maximum strength, while avoiding weaker areas. This approach will lead to a reduction of postoperative complications resulting from the deterioration of fixation (eg, cut-out, migration of osteosynthesis material, etc).[29–31]

Currently, CT scanning appears to be the most suitable investigation for obtaining large amounts of data, being readily available and relatively cost-effective. This technique has been shown to be useful in the study of trabecular patterns.[32,33] A detailed map of the trabecular system at the proximal femur level using data obtained through CT scans represents a useful tool for the assessment of the modifications of bone density. CT imaging enables the creation of complex models that can be subsequently used for finite element analysis simulations.[7,34,35]

It is well known that the femoral neck is a site of complex loading, shared between cortical and trabecular compartments, and pre-existing osteoporosis further increases the risk of a femoral neck fracture after falls. Within the proximal femur, the trabecular system provides a specific distribution that allows it to support the body's weight. Two main forces act on the proximal femur: one on the femoral head and the other on the greater trochanter, while the architecture of the trabecular system resembles that of Gothic cathedrals.[36,37] The organization of the trabecular system in the proximal femur manages to provide maximum strength with minimal mass.[38] Several studies have demonstrated that the way various forces act at the hip level influences the trabecular system, which adapts to the stresses it experiences, thereby reaffirming Wolff's law once again.[39–45]

The aim of our study was: 1) to create a map of changes in CT radiodensity in the right proximal femur in patients with various degrees of osteoporosis; 2) to quantify the differences between the various anatomical regions of interest and 3) to follow the evolution of these changes as the disease progresses to osteopenia or/and to advanced osteoporosis. A detailed statistical analysis was employed to confirm these modifications, supplemented with correlations with previously known results regarding the major trabecular structures. Our assessments were mainly focused on the trabecular bone, but an additional investigation of the modifications of the maximum density of the metaphyseal cortical bone was also performed.

Materials and Methods

Patient Characteristics

In this retrospective study, 77 right hip CT scans acquired between 2014 and 2023 were selected from the database of the Orthopedic department of the Emergency County Clinical Hospital, Oradea, Romania. The CT scans were performed using the GE Optima CT520 and the GE Revolution EVO scanners (GE HealthCare, Chicago, Illinois), with slice spacing ranging from 0.6 to 1.25 mm and resolution per pixel of 0.7–0.95 mm.

The study was approved by the Institutional Review Board and Ethical Council of the Emergency County Clinical Hospital, Oradea, Bihor - Romania (no. 39135/09.01.2023 and 39657/15.01.2023). Since the current work is a retrospective study, the patients' consents were not necessary as the medical records were anonymized, ensuring the

privacy of the participants. The research was conducted in compliance with the Declaration of the World Medical Association of Helsinki.

The patients were divided into 3 groups based on the radiological features, namely healthy patients (H), patients diagnosed with osteopenia (OP) and patients diagnosed with advanced osteoporosis (AO). The grouping of patients was performed based on the Hounsfield Unit (HU) values at the level of the femoral neck. Thus, patients with predominant values of HU>150 in the spongy bone were considered to have normal bone density, while those with frequent values of HU<100, were categorized into the "advanced osteoporosis" group. The patients with frequent HU values above 150 but presenting areas with negative HU values were included in the "osteopenia" group. In the same group we also included patients with variable HU values (80–180) that did not meet the criteria for the "normal" or the "advanced osteoporosis" groups.

Exclusion criteria: patients with fractures in the proximal third of the femur, patients with bone tumors, geodes, advanced coxarthrosis, or other pathologies leading to the loss of femoral head sphericity or the development of large osteophytes. After applying the exclusion criteria, 51 patients remained in the study. Our analysis was focused on two planes that were visually centered on the femoral head and neck when seen from below (longitudinal slices) and respectively from the side (oblique slices). The demographic characteristics and distribution of HU units according to each group, are presented in Tables 1 and 2, where HU was calculated by considering a spatial mean value only inside the trabecular region. SD represents the standard deviation.

Image Processing

The cross sections of the right femurs were obtained in 3D Slicer version 5.2.2 r31382/fb46bd1 (https://www.slicer.org/), by re-slicing the images and selecting a longitudinal and oblique slice corresponding to the planes that are centered on the femoral head and neck observed from below and respectively from the side. The images were then cropped and warped in Fiji version 2.14.0/1.54f, GNU General Public License, (https://imagej.net/software/fiji/downloads),[46] by applying the thin plate spline method using the BigWarp plugin[47] and using a healthy femur as size and shape reference, so that they overlap sufficiently well for further comparative analysis. Major anatomical landmarks were used in the warping process, as described in Spatial Figureping.

Table 1 Demographic Characteristics of the Patients Divided in Three Groups

Parameter	Group		
	H	OP	AO
Age (mean value ±SD)	27.5 ± 7.0	54.0 ± 14.6	77.1 ± 8.6
Female N (%)	6 (54.5)	9 (47.4)	13 (61.9)
Male N (%)	5 (45.5)	10 (52.6)	8 (38.1)
HU lateral section average (min/max/SD)	268 (209/374/47)	183 (130/222/27)	105 (31/187/47)
HU oblique section average (min/max/SD)	327 (260/417/53)	232 (165/303/37)	151 (60/236/56)

Table 2 Mean HU Values According to Age Distribution

Parameter	Age Group		
	<50 y	50–70 y	≥70 y
Female N (%)	8 (47.1)	9 (56.3)	11 (61.1)
Male N (%)	9 (52.9)	7 (43.7)	7 (38.9)
HU lateral section average (min/max/SD)	239 (156/374/56)	162 (63/222/45)	109 (31/208/54)
HU oblique section average (min/max/SD)	298 (219/417/59)	209 (100/303/52)	154 (60/248/61)

Statistical Analysis

Statistical analysis has been performed by extracting image information, such as the average image intensity values for various anatomical regions of interest using Fiji macros, followed by statistical processing in the Microsoft Office Excel 12.0, MathWorks Matlab R2016b and OriginLab OriginPro 8.5 software. The spatial cross sections were plotted using the Fiji software. Error bars have been obtained in Microsoft Office Excel from the standard deviations of both the healthy and osteoporotic/osteopenic femur distributions using small error approximations. The statistical significance of the differences between the spatial means of various anatomical regions of interest has been assessed in Matlab by finding the p-values of pairwise Student's *t*-tests and using the same software to represent the final results as heat maps of the p-values, without applying any corrections for multiple comparisons. To compare pairs of regions, the distribution of region 1 (of each pair) for the normal femurs was scaled by either the ratio or the absolute difference between the average diseased femur and the average normal femur in region 2 (of the same pair) and then compared with the distribution in region 1 for the diseased femurs using a Student's *t*-test. For each such pair of regions, only the largest p-value was retained when switching the roles of regions 1 and 2. The dendrograms corresponding to the heat maps (representing the differences of the mean values between the various anatomical regions) were obtained with the Matlab software applying the single linkage method and Euclidean distances. Pearson correlations between the radiodensity of healthy femur regions and the degree of osteoporosis were obtained using the OriginPro software.

Results

Spatial Mapping

Major landmarks used in the warping process were as follows: the epiphyseal line and greater trochanter growth plate; the principal compressive group; the neck-shaft angle; the coordinates of the femoral neck and greater trochanter. The thickness of the femoral neck was chosen as a visual guide for the vertical scale in the longitudinal slices (Figure 1).

The useful areas in the final 16-bit grayscale images have 112×94 pixels for the longitudinal sections and 91 × 25 pixels for the oblique sections, representing the radiodensity expressed in HU. The average cross sections corresponding to the three patient groups are shown in Figure 2, with the longitudinal cross sections in the first row (Figure 2a–c) and the oblique cross sections in the second row (Figure 2d–f).

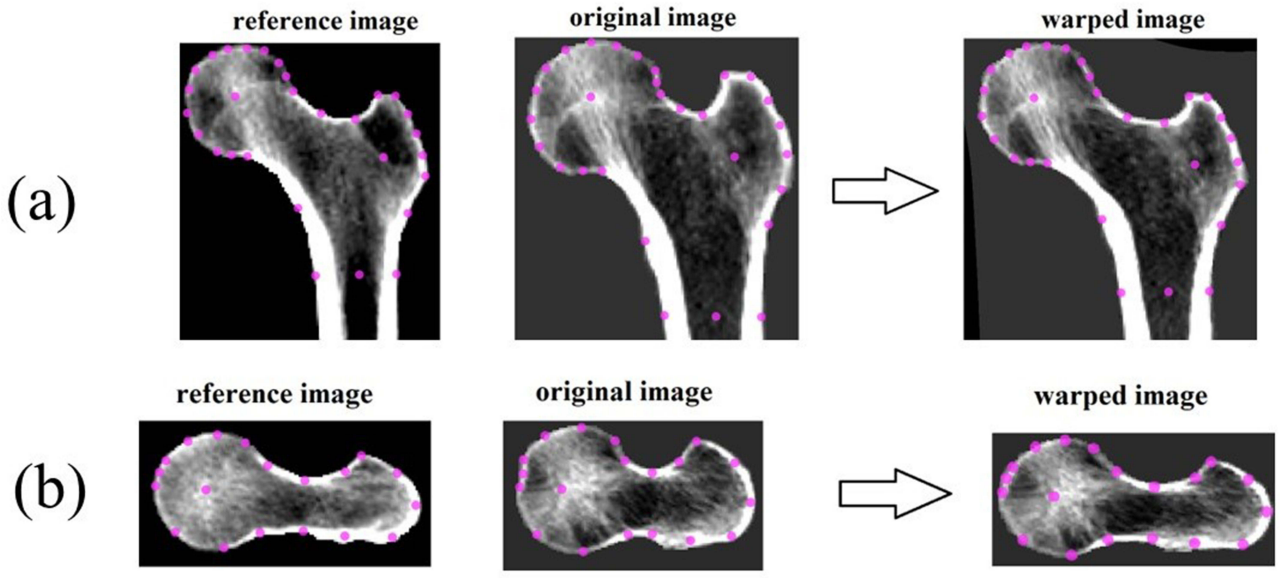

Figure 1 Warping process example for longitudinal (**a**) and the corresponding oblique slices (**b**), using a healthy femur as reference and warping a femur with advanced osteoporosis (original image). Gray levels and spatial scales of various images have been auto-scaled for best viewing and are not comparable. The oblique sections in (**b**) correspond to the oblique center line running through the femoral head and neck in (**a**), perpendicular to its plane.

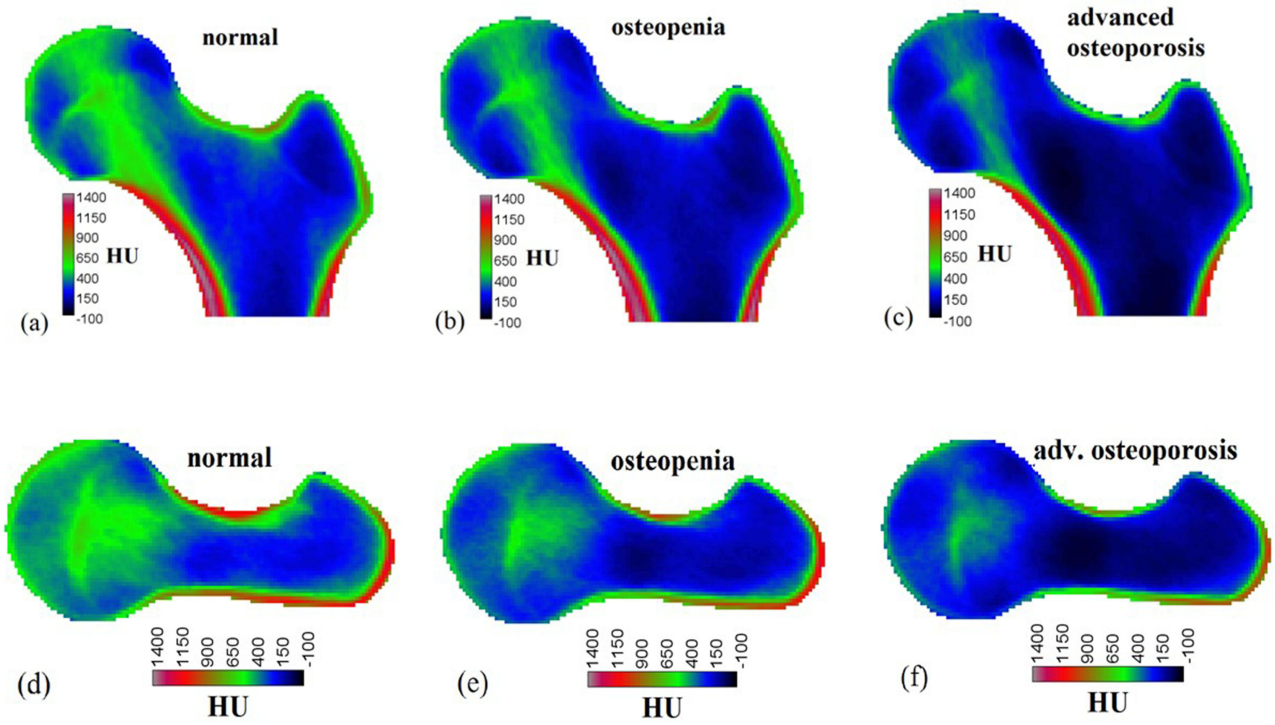

Figure 2 Average femur CT cross section for healthy patients (**a** and **d**), patients diagnosed with osteopenia (**b** and **e**) and patients with advanced osteoporosis (**c** and **f**). The color scales represent HU.

In order to evaluate the spatial evolution of osteoporosis, we represented the percentage of the relative decrease in radiodensity of the average osteoporotic/osteopenic femur compared to the average healthy femur (Figure 3) as well as the absolute decrease in HU (Figure 4). It should be noted that although the radiodensity is correlated with bone density, there is not a simple relationship between them, due to the presence of soft tissue in addition to the bone. We noticed that a major relative resorption of bone occurs in the Ward triangle, while the relative resorption in the principal compressive group and cortical bone of the metaphysis is less visible. This is in agreement with the Singh index criteria for osteoporosis,[22] according to which the Ward triangle becomes preeminent in the initial phases and the principal compressive group disappears last. We also note that in general, the regions of high radiodensity tend to undergo a smaller relative decrease of radiodensity as the disease progresses, while regions of low radiodensity undergo a larger relative decrease of radiodensity. In other words, the anatomic regions that are naturally subjected to less stress in accordance to Wolff's law, are more affected than those subjected to high stress.

According to Figure 4, the maximum absolute decrease in radiodensity is not concentrated on the Ward triangle, but shifted towards the nearby inferior-posterior compact bone. In the longitudinal section, at the level of the intertrochanter and trochanter, we noticed a lower absolute decrease in radiodensity compared to the femoral neck; moreover, the top of the femoral head was also less affected compared to the surrounding regions. When considering the oblique section, again, the intertrochanteric region seems less affected than the femoral neck, especially in the advanced stage of osteoporosis. Generally, in the oblique section, the bone resorption appears asymmetrical in the anterior-posterior direction.

We analyzed the spatial evolution of osteoporosis (Figure 5) in 10 representative regions for both sections, labeled A-J (Figure 5a) and K-T respectively (Figure 5c). The size of the trabecular regions A-I, K-T was chosen large enough to account for inaccuracies in the choice of the landmark points during the warping process. In the longitudinal section, region A is bounded by the epiphyseal line and the principal compressive group, corresponding to a region in the Babcock triangle; regions B and D correspond to the triangles obtained from the intersection of the principal compressive group and the epiphyseal line; region C corresponds to the principal compressive group, while region E corresponds to the remaining area in the femoral head, below the epiphyseal line. Region F corresponds to

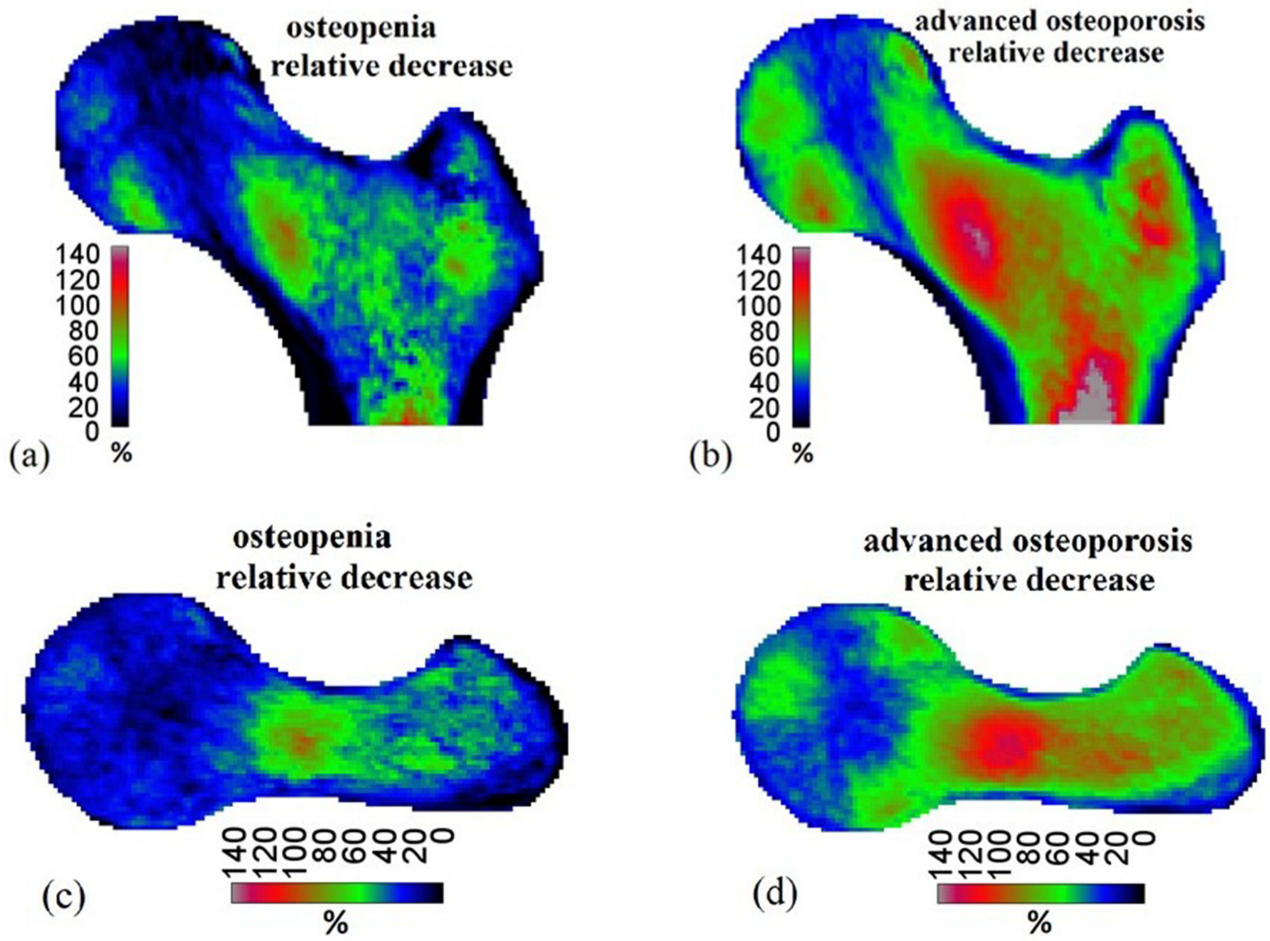

Figure 3 Average spatial distribution of osteopenia (**a** and **c**) and advanced osteoporosis (**b** and **d**), displayed as the relative decrease in radiodensity.

an area overlapping the Ward's triangle, region G to the remaining area in the femoral neck, region H corresponds to the greater trochanter, above the growth plate, region I to the intertrochanter and, finally, region J corresponds to the region in the metaphysis, where cortical bone was investigated. In all the regions except J, only the trabecular bone was subjected to analysis. The reason for performing the cortical bone analysis only in region J was related to the intrinsic resolution of the CT scanner which leads to inaccurate values. Since the accurate alignment of the rather thin cortical bone in region J is difficult to achieve during the warping process, only the maximum radiodensity value in region J has been considered, while in the trabecular regions the spatial mean of radiodensity was investigated.

In the oblique section, region K is centered on the femoral head, and represents a high density region corresponding to the intersection between the principal compressive group and the principal tensile group. Regions L and P are located in the femoral head, being bounded to the left by the epiphyseal line, while regions M, N, O are located on the other side of the epiphyseal line, their outlines being guided by the location of features of interest, respectively the anatomical regions of high or low intensity presented in Figures 2d–f, 3c and d). Region Q is located in the remaining area of the femoral head, region R overlaps Ward's triangle, region S covers some of the remaining region in the femoral neck and region T is located in the intertrochanter.

A statistical approach was employed in order to evaluate the changes of the mean values of radiodensity in the anatomical regions A-I, K-T and of the maximum values of the radiodensity in the region J. Additionally, a comparison between various anatomical regions in terms of osteoporosis evolution was evidenced.

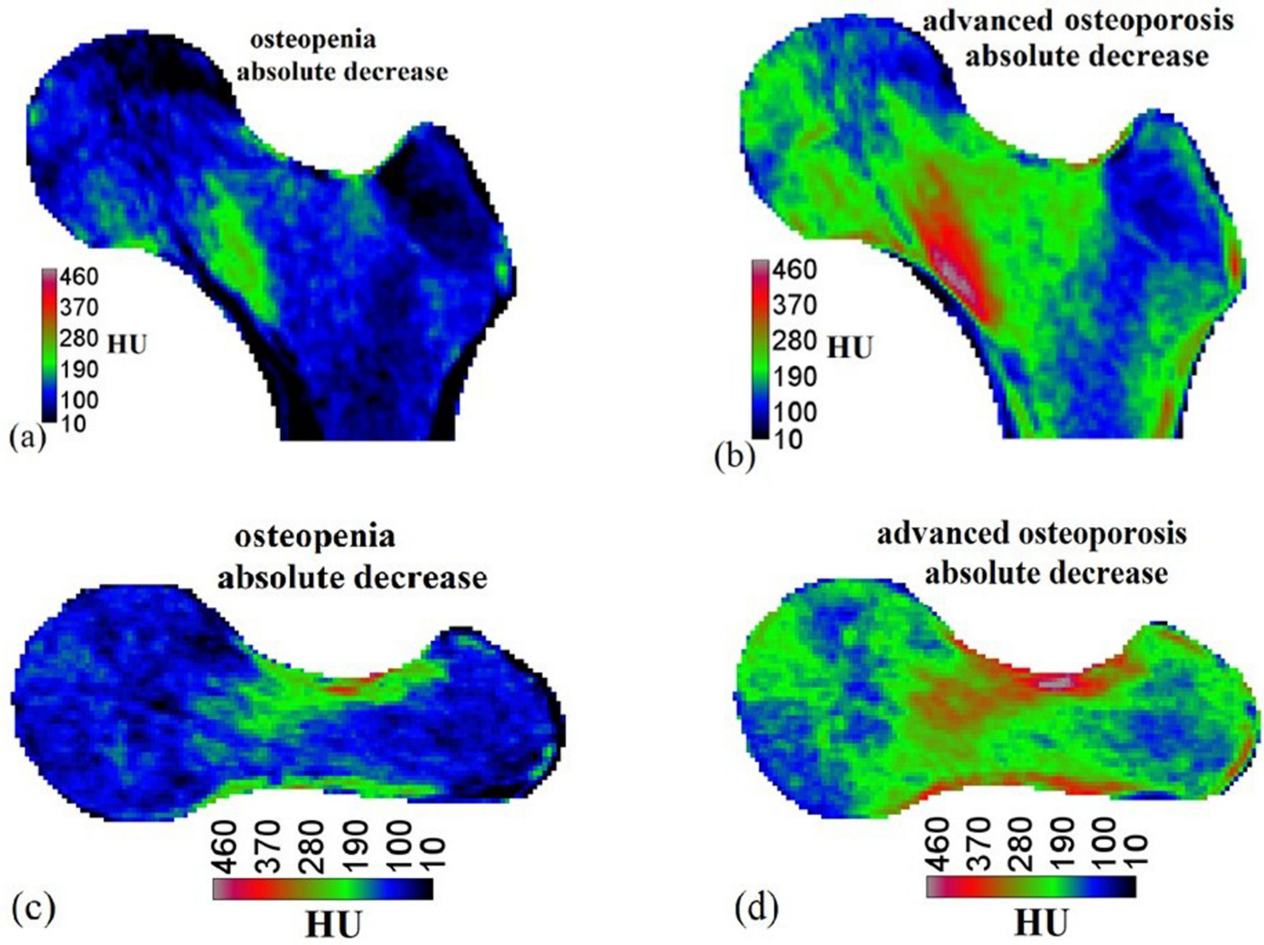

Figure 4 Average spatial distribution of osteopenia (**a** and **c**) and advanced osteoporosis (**b** and **d**), displayed as absolute decrease in radiodensity, measured in HU.

Statistical Analysis of the Relative Decrease of Radiodensity

In Figure 6 we represent the relative decrease in radiodensity of diseased femurs relative to healthy ones, for all 10 regions. Error bars have been obtained from the standard deviations of both the normal and diseased femur distributions using the low error approximation for fractions. Some error bars are shown only on the positive half of the y-axis. Since the radiodensity can reach negative HU values, some percentages can exceed 100.

In the longitudinal section, it can be observed that the smallest resorption occurs in regions C and J, namely the principal compressive group and the cortical bone, while region F, corresponding to the Ward triangle, is affected by the largest resorption. We would like to point out that even though the maximum value for cortical bone in region J is affected the least, the thickness of the cortical bone in this region may vary. The amount of relative decrease also depends on the size of the chosen region. For instance, a smaller region F would undergo a larger mean relative decrease in radiodensity in Figure 6a. The trochanter region exhibits small size focal spots in the advanced stage (Figure 3b), which might be due to the inaccurate alignment during the warping process. Similarly, in the oblique section, the region K (with the highest density) undergoes the smallest relative resorption, followed by regions O and M, while region R corresponding to the Ward triangle, undergoes the largest resorption.

Figures 7a, b, 8a and b) represent the p-values (*t*-test) heat map of the spatial distribution of radiodensity in the case of moderate, respectively advanced osteoporosis. The diagonal values compare the mean radiodensity of the healthy and osteoporotic femurs related to the selected regions of interest. The off-diagonal elements verify whether the difference of the corresponding pair of regions is statistically significant, when osteoporosis is measured by the relative decrease in radiodensity, p-values < 0.001 being represented as 0.001.

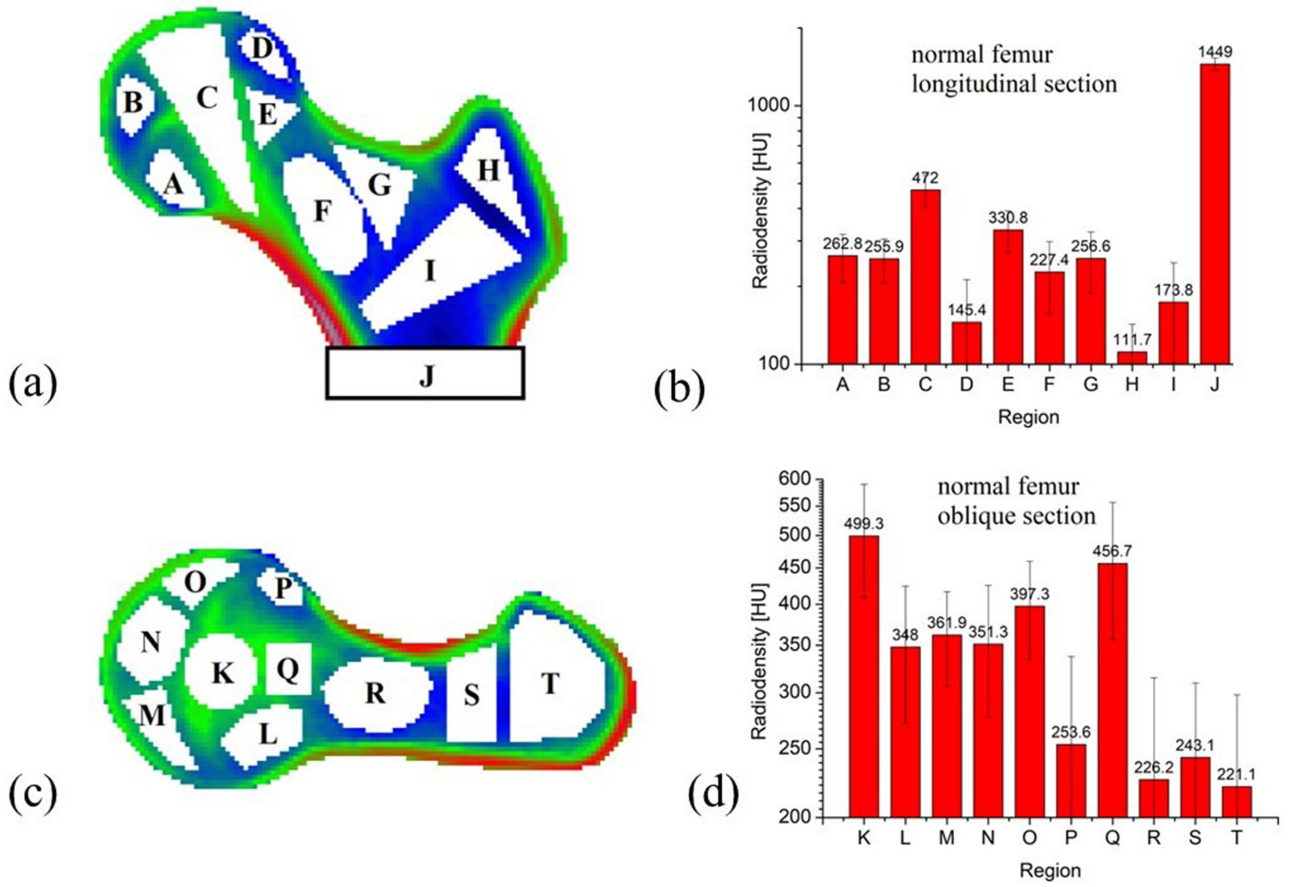

Figure 5 Analyzed anatomical regions, shown as white areas superimposed onto the average healthy femur (**a** and **c**). The histograms show the average normal bone radiodensity and corresponding standard deviations for the analyzed regions (**b** and **d**). The features of trabecular bone were investigated in the regions A-I and K-T, while the cortical bone in region J.

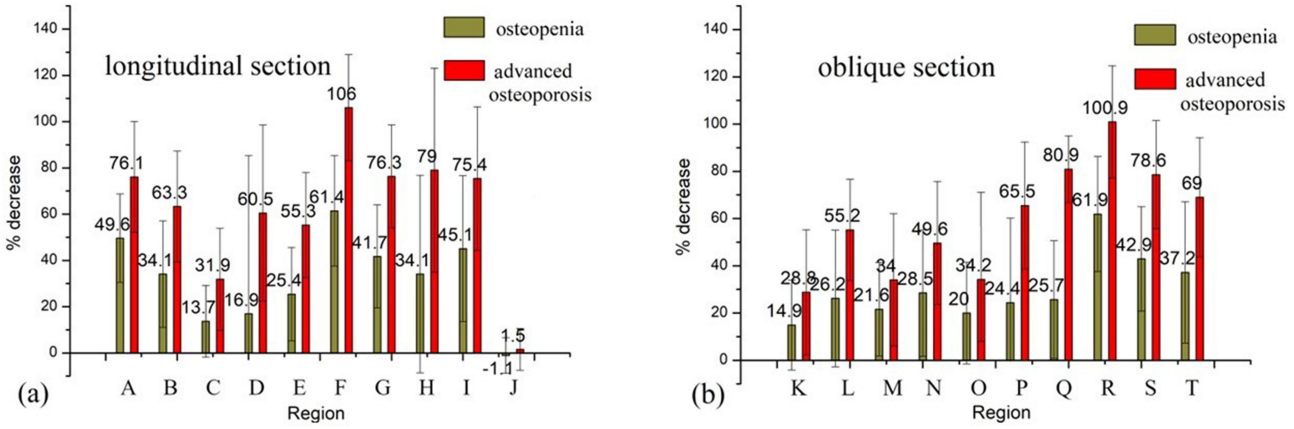

Figure 6 Relative decrease in radiodensity of femurs with moderate and advanced osteoporosis, in the longitudinal (**a**) and oblique (**b**) sections.

The dendrograms compare the means of the osteoporosis distribution within the various anatomical regions, being useful in revealing the particular regions with a similar degree of resorption. Typically, pairs of regions with very different means will have a small p-value and vice-versa. The maximum value on the linear vertical scale of the dendrograms is also indicated for reference.

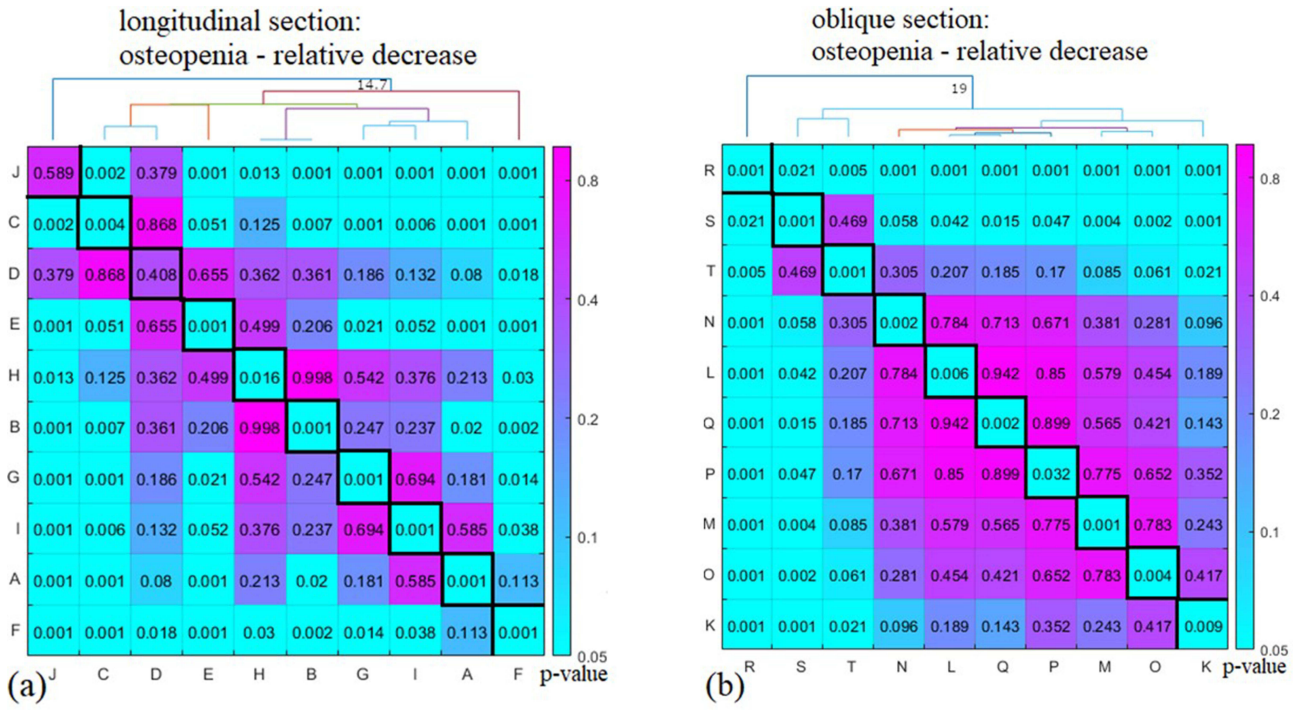

Figure 7 p-values heat map (log scale) of the spatial distribution of osteopenia, measured by the relative decrease in radiodensity in the various anatomical regions, in the longitudinal (**a**) and oblique (**b**) sections. The dendrograms compare the means of the spatial distribution of osteopenia in the various regions.

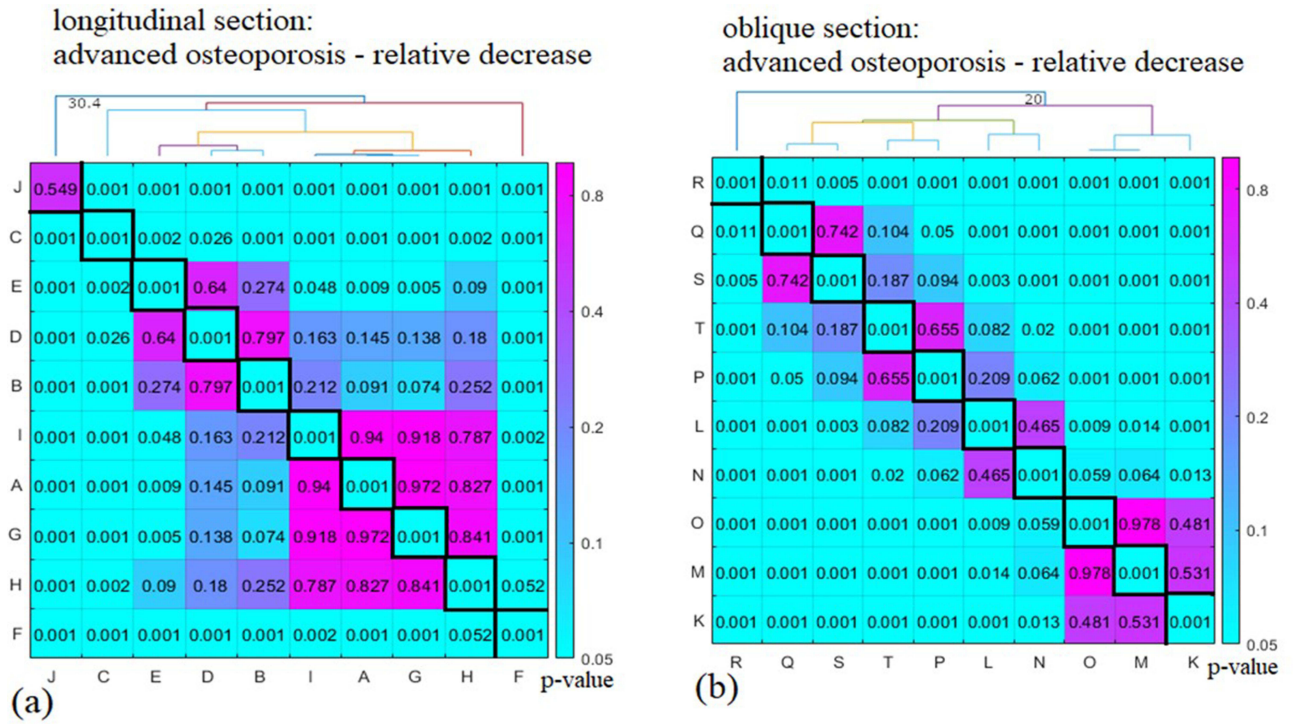

Figure 8 p-values heat map (log scale) of the spatial distribution of advanced osteoporosis, measured by the relative decrease in radiodensity in the various anatomical regions in the longitudinal (**a**) and oblique (**b**) sections. The dendrograms compare the means of the spatial distribution of advanced osteoporosis in the various regions.

From the diagonal values presented in Figure 7a and b) we notice that the radiodensity in healthy and osteopenic femurs differs significantly in all the regions except D and J. Considering the longitudinal slices, significant differences were observed when comparing the principal compressive group with other regions: region C differs significantly from

all but regions D and H. On the other hand, region F (the Ward triangle), differs significantly from all but region A. Cortical bone radiodensity differs meaningfully from all but region D. Considering the oblique slices, region R (which overlaps the Ward triangle) differs significantly from all other regions, while region K (with maximum density in the femoral head) differs significantly from the regions R, S, T outside the femoral head.

According to the values presented in Figure 8a and b), when osteoporosis evolves to the advanced stage we notice a higher number of p-values that are roughly equal or below the 0.05 significance level, the differences becoming thus more pronounced and statistically significant. Considering the longitudinal sections, healthy and osteoporotic femurs differ in a statistically significant manner for all but region J, where the dense cortical bone undergoes very small relative change as the disease progresses. Significant differences with respect to other regions were noted in the principal compressive group (region C), the cortical bone (region J) as well as the Ward triangle (region F). Considering the oblique sections, the maximum density in region K differs significantly from all but regions O and M (which are the 3rd respectively the 4th densest regions in the oblique sections of the healthy femur represented in Figure 5d) and undergo the least relative decrease after region K.

Statistical Analysis of the Absolute Decrease in Radiodensity

In Figure 9a and b we represent the absolute decrease in radiodensity for the 10 anatomical regions, along with the appropriate error bars obtained from the standard deviations of both the normal and osteoporotic/osteopenic femur distributions by applying the low error approximation for differences.

In the longitudinal sections, in absolute terms, the decrease in region F is less pronounced than as a percentage and region C does not undergo the smallest decrease among the trabecular regions. As previously presented in Figure 5b, the healthy bone has a rather high radiodensity in region C, and relatively low value in region F. This suggests that bone resorption as a percentage has a very strong effect on region F and a very small one on region C. We also noted that cortical bone is resorbed the least both in absolute and relative terms, however its thickness may vary. The top of the femoral head, where region D is located, undergoes less resorption than the surrounding regions (see also Figures 4a and b) while the regions H and I (in the greater trochanter and intertrochanter) are less affected than the femoral neck regions F and G.

Similarly, in the oblique sections, the decrease in region R stands out less in absolute terms than as a percentage, while region K no longer presents the smallest decrease in either moderate or advanced osteoporosis. Region Q suffers the largest absolute decrease in the advanced stage, possibly influenced by its proximity to the Ward triangle. As noted in Figure 5, the maximum absolute decrease is shifted towards the nearby inferior-posterior cortical bone, and the intertrochanter suffers less absolute decrease than the adjacent femoral neck. We would like to re-emphasize that the decrease in radiodensity of the various anatomical regions also depends on the size of the selected areas.

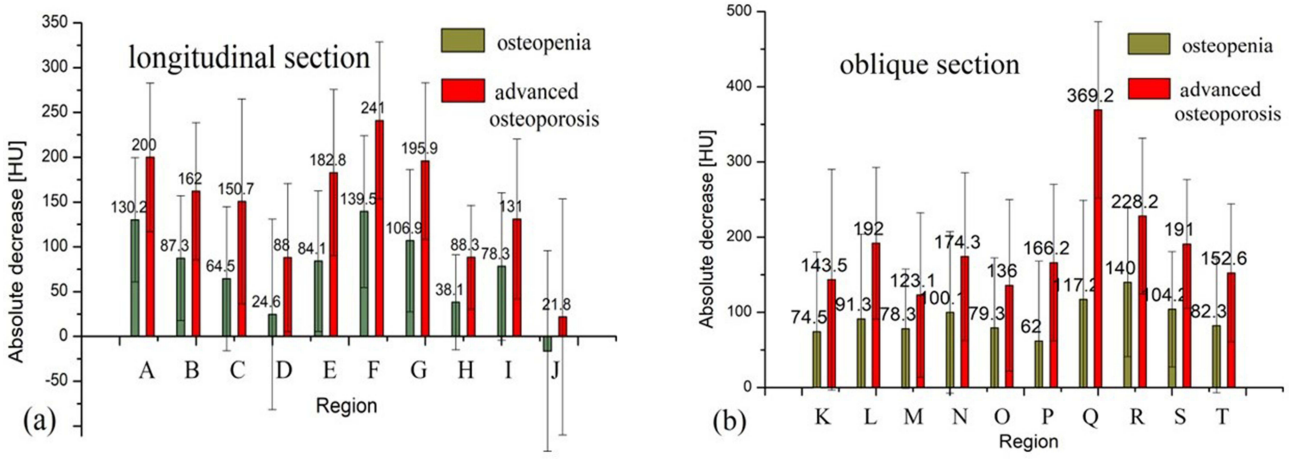

Figure 9 Absolute decrease of radiodensity in femurs with osteopenia respectively advanced osteoporosis, in the longitudinal (**a**) and oblique (**b**) sections.

In Figures 10a, b, 11a and b we represent the p-values for the differences between the various regions for osteopenia and advanced osteoporosis respectively, when measured by the absolute decrease of radiodensity. The diagonal elements are the same as in Table 3, and the off-diagonal elements verify whether the difference of the osteoporosis of the

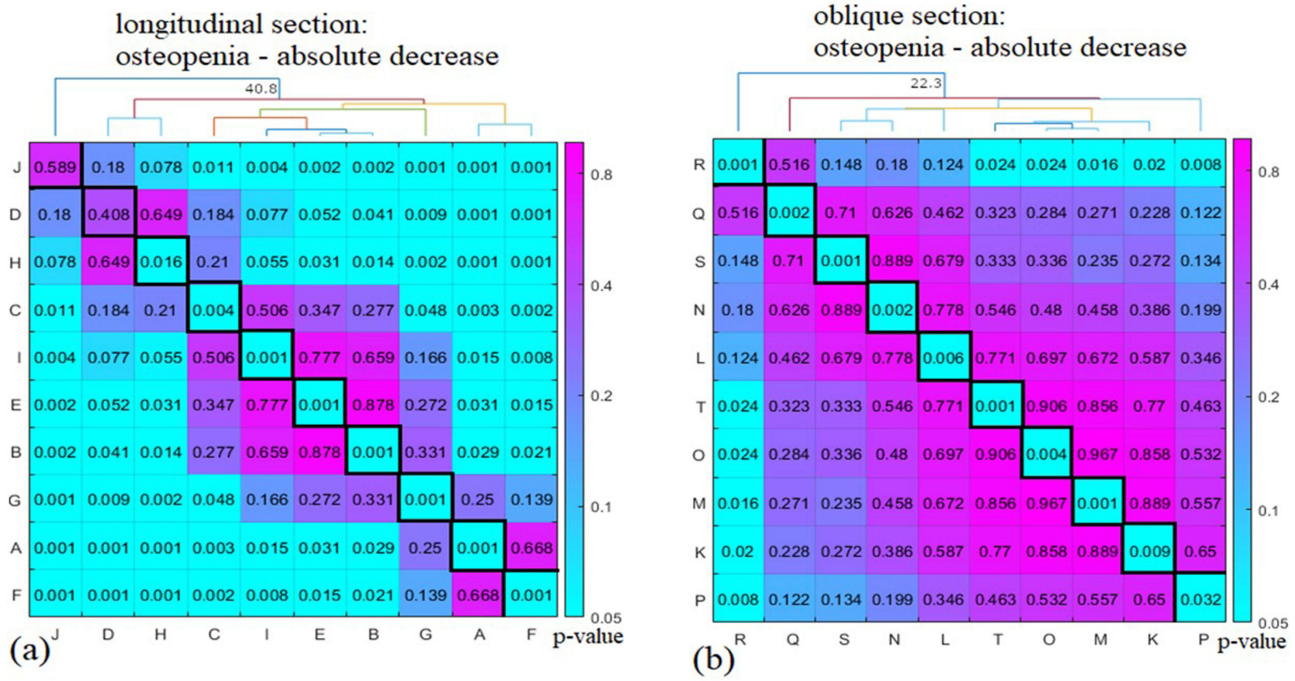

Figure 10 p-values heat map (log scale) for the spatial distribution of osteopenia as measured by the absolute decrease in radiodensity for the various anatomical regions, in the longitudinal (**a**) and oblique (**b**) sections. The dendrograms compare the means of the spatial distribution of osteopenia in the various regions.

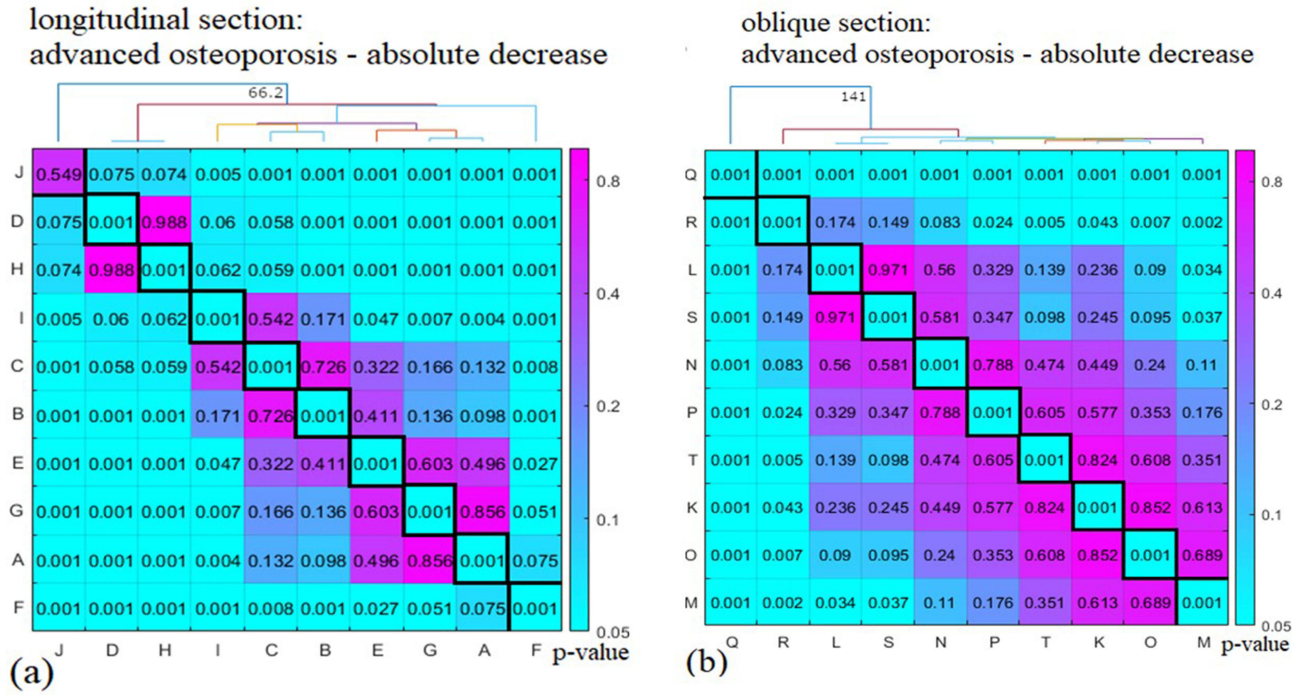

Figure 11 p-values heat map (log scale) for the spatial distribution of advanced osteoporosis as measured by the absolute decrease in radiodensity for the various anatomical regions, in the longitudinal (**a**) and oblique (**b**) sections. The dendrograms compare the means of the spatial distribution of advanced osteoporosis in the various regions.

Table 3 Pearson Correlation Coefficients (R) and Corresponding p-values for the Correlation Between the Average Normal Femur and the Spatial Distribution of Osteoporosis as Measured by the Relative Decrease in Radiodensity

Pearson Correlation: Relative Decrease in Radiodensity of Osteoporotic vs Healthy Femur	**OP**	**AO**
Longitudinal sections: all 10 regions	R=−0.67, p=0.033	R=−0.83, p=0.003
Longitudinal sections: only 9 trabecular regions	R=−0.35, p=0.36	R=−0.64, p=0.066
Oblique sections.: all 10 trabecular regions	R=−0.74, p=0.014	R=−0.61, p=0.059

corresponding pair of regions is statistically significant, when osteoporosis is measured by the absolute decrease in radiodensity. As before, all p-values less than 0.001 have been represented as 0.001.

Once again, we can notice the increase in the number of regions with small p-values, and the differences become more important when the disease progresses. Both the maps for relative and absolute spatial changes clearly reveal statistical differences between various regions of the bone, thus proving that osteoporosis affects different regions in a different manner.

In the longitudinal sections, region F differs significantly from almost all other regions, excepting regions A and G, and so does region J, with the exception of regions D and H. Region D (inside the upper part of the femoral head) differs significantly from most of the surrounding regions (A, B in osteopenia, respectively A, B, E in advanced osteoporosis), however its difference from the adjacent region C is not significant. In terms of absolute decrease, the trochanter region H differs meaningfully from the regions in the femoral neck. However, the selected intertrochanter region I differs meaningfully from the femoral neck region G only in the advanced stage of osteoporosis. In the oblique sections, the intertrochanter region T only differs meaningfully from region R, but not from S. Region Q differs meaningfully from all other regions in the advanced stage (see also Figure 4d). Region R differs from most other regions, with four exceptions in osteopenia (namely L, N, Q, S) and 3 exceptions in advanced osteoporosis (namely L, N, S).

Statistical Analysis of Correlation with Normal Radiodensity (Healthy Femur)

Pearson correlation coefficients between the radiodensity of the various regions in the average normal femur and the spatial distribution of osteoporosis were determined in order to check whether the statistical analysis confirms that the regions with higher radiodensity are less affected by osteoporosis and vice-versa (Table 3).

When osteoporosis was measured by the absolute decrease in radiodensity, the correlation did not achieve statistical significance ($p > 0.05$). However, when measured by the relative decrease in radiodensity, we found a strong correlation coefficient for advanced osteoporosis in the longitudinal sections (R=−0.83, p-value=0.003), while a lower correlation was obtained if only the regions of trabecular bone were considered (R=−0.64, p-value=0.066). For osteopenia, the correlation is determined by the outlier point corresponding to region J and is thus not noteworthy (as shown in Figure 12a and b). In the oblique sections, a better correlation (R=−0.74, p-value=0.014) was noted for osteopenia than for advanced osteoporosis (R=−0.61, p-value=0.059). The graphical representation of the correlation between normal radiodensity and relative decrease in radiodensity of osteoporotic femurs is presented in Figure 8, considering both longitudinal and oblique sections.

The results clearly indicate that higher radiodensity regions in the normal femur tend to undergo less relative resorption in osteoporosis and vice-versa, which is mostly evident in the oblique section. This fact is mainly a result of the normalization to the average normal femur radiodensity and thus, an absolute radiodensity decrease will have a higher impact on the low radiodensity regions, as noted in.[23]

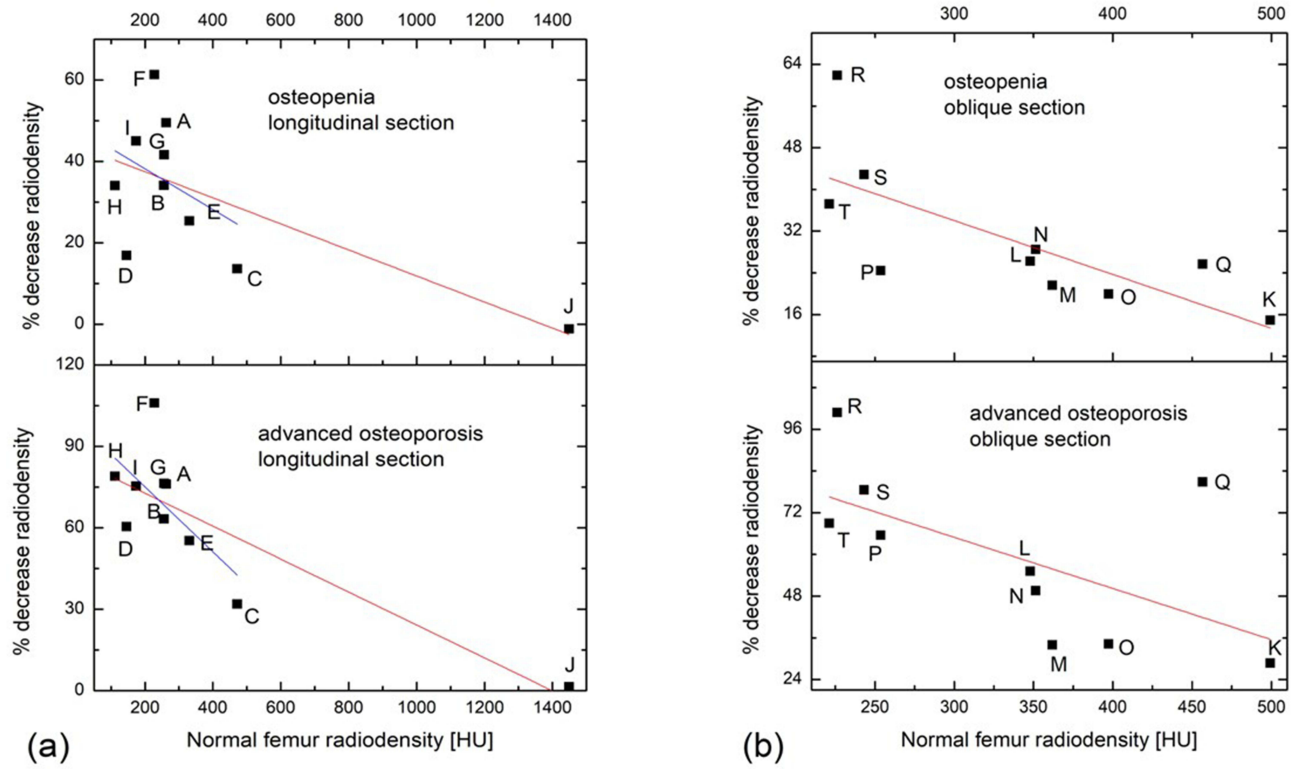

Figure 12 Correlation between normal femur radiodensity and relative decrease radiodensity in osteoporotic femurs, in the longitudinal (**a**) and oblique (**b**) sections. The various regions are indicated with capital letters. The red lines represent the best linear fit for all 10 regions while the blue lines in panel (**a**) consider only the 9 trabecular regions.

Discussion

In this work, we investigated the spatial evolution of osteoporosis in the right proximal femur, from the normal, healthy stage, to the moderate (osteopenia) and then the advanced osteoporosis stage and fully quantified the spatial decrease in radiodensity during this progression. Two perpendicular sections through the proximal femur were considered and a detailed map of the evolution was generated both in terms of relative and absolute decrease in radiodensity. Each section was divided into 10 anatomical regions of interest, which were selected through direct observation of the images obtained from the overlays and subsequently correlated with Ward's description of the trabecular system.[48,49] Previous authors attempting to study the properties of the trabecular system have usually chosen to investigate between 3 and 7 areas of the proximal femur, without being able to provide a detailed spatial map.[18,27,50–53]

Since authors who focused on the evolution of cortical bone have found that it was challenging to accurately delineate the cortical bone at the level of the femoral head and neck,[54] its thickness and density were not subjected to our analysis. In addition, subchondral bone undergoes more significant demineralization.[55]

The major trabecular regions of the proximal femur are known to change in size with demineralization. Radiologically, the first areas to demineralize are the secondary tension and compression groups and the greater trochanter group. Ward's triangle increases its surface area.[22,23] The primary compressive system, which bears the majority of the forces and has a density similar to cortical bone, demineralizes the slowest.[33]

When measured in terms of relative decrease in radiodensity, we found that the anatomical regions with high radiodensity are less affected by osteoporosis than the low radiodensity ones. Thus, among the trabecular regions, the Ward triangle is more susceptible to weakness (as radiodensity decreased by an average 61–62% in osteopenia and 101–106% in advanced osteoporosis), while the principal compressive group is less prone to deterioration (radiodensity decreased by an average 14–15% in osteopenia and 29–32% in advanced osteoporosis). These findings are in agreement with Singh's semiquantitative method for determining the stages of osteoporosis,[22] and provide a possible explanation for the high relative frequency of fractures in the femoral neck.[5] We found statistically significant differences in the absolute

variation of radiodensity as osteoporosis progresses, although the absolute bone resorption is not correlated with the normal radiodensity, while previously, no evidence of selective absolute bone loss was found.[23] The maximum absolute decrease in radiodensity is not concentrated in the Ward triangle, but shifted towards the nearby inferior-posterior edge of the bone. Inside the femoral head, the upper region undergoes a minimal absolute decrease, especially in the advanced stage. The greater trochanter trabecular bone presents a lower absolute decrease compared to the femoral neck. The maximum density of metaphyseal cortical bone does not change significantly in either absolute or relative terms, however its thickness may decrease.[11,18,56] A statistical comparative analysis of the various regions showed that the differences between the modifications that occurred in the various regions become more statistically significant as the disease progresses to the advanced stage. Our quantitative interpretation of the spatial evolution of osteoporosis could serve as an input for further finite element simulations of femoral fractures and fixation methods, as we noticed a gap in the available literature in this regard.

Conclusions

From our image analysis based on the computational re-slicing and warping of CT scan images of patients with various degrees of osteoporosis, we were able to create a spatial map of the modifications produced by the disease in terms of the reduction in radiodensity in the proximal femur. The quantification of these changes was performed by applying a comparative statistical analysis, taking into account different anatomical regions, which revealed increasingly significant differences as osteoporosis progresses.

In relative terms, the Ward triangle is affected the most and the principal compressive group the least, while in absolute terms, the maximum decrease in radiodensity is shifted towards the inferior-posterior side of the bone, the greater trochanter is affected less than the femoral neck and inside the femoral head, the upper region undergoes a minimal absolute decrease, especially in the advanced stage of osteoporosis. The emerging patterns and quantitative interpretation of the spatial evolution of osteoporosis could serve as a valuable input for further finite element simulations of femoral fractures and for the optimization of fixation methods.

Institutional Review Board Statement

The study was conducted in accordance with the Declaration of Helsinki, and approved by the Institutional Review Board and Ethical Council of the Emergency County Clinical Hospital, Oradea, Bihor, Romania (no. 39135/09.11.2023 and 39657/15.11.2023).

Data Sharing Statement

All data are available in the County Emergency Clinical Hospital of Oradea-Romania, Department of Orthopedics and Traumatology.

Author Contributions

All authors made a significant contribution to the work reported, whether that is in the conception, study design, execution, acquisition of data, analysis and interpretation, or in all these areas; took part in drafting, revising or critically reviewing the article; gave final approval of the version to be published; have agreed on the journal to which the article has been submitted; and agree to be accountable for all aspects of the work.

Funding

This research was supported by the University of Oradea, Faculty of Medicine and Pharmacy.

Disclosure

The authors declare no conflicts of interest in this work.

References

1. Waddell JP. *Fractures of the Proximal Femur: Improving Outcomes: Expert Consult: Online and Print*. 1st ed. Philadelphia, PA: Saunders; 2010.
2. Moreland BL, Legha JK, Thomas KE, Burns ER. Hip fracture-related emergency department visits, hospitalizations and deaths by mechanism of injury among adults aged 65 and older, United States 2019. *J Aging Health*. 2023;35:345–355. doi:10.1177/08982643221132450
3. Greenspan SL, Myers ER, Maitland LA, Resnick NM, Hayes WC. Fall severity and bone mineral density as risk factors for Hip fracture in ambulatory elderly. *JAMA*. 1994;271:128–133. doi:10.1001/jama.1994.03510260060029
4. Lewis SR, Macey R, Stokes J, Cook JA, Eardley WG, Griffin XL. Surgical interventions for treating intracapsular Hip fractures in older adults: a network meta-analysis. *Cochrane Database Syst Rev*. 2022;2022:CD013404. doi:10.1002/14651858.CD013404.pub2
5. Beck A, Rüter A. Schenkelhalsfrakturen-Diagnostik und therapeutisches Vorgehen. *Unfallchirurg*. 1998;101:634–648. doi:10.1007/s001130050317
6. Bettamer A, Hambli R, Allaoui S, Almhdie-Imjabber A. Using visual image measurements to validate a novel finite element model of crack propagation and fracture patterns of proximal femur. *Comput Methods Biomech Biomed Eng Imaging Vis*. 2017;5:251–262. doi:10.1080/21681163.2015.1079505
7. Mirzaei M, Samiezadeh S, Khodadadi A, Ghazavi MR. Finite element prediction and experimental verification of the failure pattern of proximal femur using quantitative computed tomography images. *Int J Biomed Biol Eng*. 2012;6:208–214.
8. Lotz JC, Cheal EJ, Hayes WC. Fracture prediction for the proximal femur using finite element models: part II--nonlinear analysis. *J Biomech Eng*. 1991;113:361–365. doi:10.1115/1.2895413
9. Peck WA. Consensus development conference: diagnosis, prophylaxis, and treatment of osteoporosis. *Am J Med*. 1993;94:646–650. doi:10.1016/0002-9343(93)90218-e
10. Ward KA, Pearse CM, Madanhire T, et al. Disparities in the prevalence of osteoporosis and osteopenia in men and women living in Sub-Saharan Africa, the UK, and the USA. *Curr Osteoporos Rep*. 2023;21:360–371. doi:10.1007/s11914-023-00801-x
11. Poole KES, Skingle L, Gee AH, et al. Focal osteoporosis defects play a key role in Hip fracture. *Bone*. 2017;94:124–134. doi:10.1016/j.bone.2016.10.020
12. Ascenzi M-G, Hetzer N, Lomovtsev A, Rude R, Nattiv A, Favia A. Variation of trabecular architecture in proximal femur of postmenopausal women. *J Biomech*. 2011;44:248–256. doi:10.1016/j.jbiomech.2010.10.017
13. Riggs BL, Melton Iii LJ, Robb RA, et al. Population-based study of age and sex differences in bone volumetric density, size, geometry, and structure at different skeletal sites. *J Bone Miner Res*. 2004;19:1945–1954. doi:10.1359/JBMR.040916
14. Tang H, Di W, Qi H, et al. Age-related changes in trabecular bone score and bone mineral density in Chinese men: a cross-sectional and longitudinal study. *Clin Interv Aging*. 2022;17:429–437. doi:10.2147/CIA.S358951
15. Thomas CDL, Mayhew PM, Power J, et al. Femoral neck trabecular bone: loss with aging and role in preventing fracture. *J Bone Miner Res*. 2009;24:1808–1818. doi:10.1359/jbmr.090504
16. Whitmarsh T, Otake Y, Uemura K, Takao M, Sugano N, Sato Y. A cross-sectional study on the age-related cortical and trabecular bone changes at the femoral head in elderly female Hip fracture patients. *Sci Rep*. 2019;9:305. doi:10.1038/s41598-018-36299-y
17. Chen H, Zhou X, Fujita H, Onozuka M, Kubo K-Y. Age-related changes in trabecular and cortical bone microstructure. *Int J Endocrinol*. 2013;2013:e213234. doi:10.1155/2013/213234
18. Nicks KM, Amin S, Melton LJ, et al. Three-dimensional structural analysis of the proximal femur in an age-stratified sample of women. *Bone*. 2013;55:179–188. doi:10.1016/j.bone.2013.02.009
19. Ito M, Wakao N, Hida T, et al. Analysis of Hip geometry by clinical CT for the assessment of Hip fracture risk in elderly Japanese women. *Bone*. 2010;46:453–457. doi:10.1016/j.bone.2009.08.059
20. Ito M, Nakata T, Nishida A, Uetani M. Age-related changes in bone density, geometry and biomechanical properties of the proximal femur: CT-based 3D Hip structure analysis in normal postmenopausal women. *Bone*. 2011;48:627–630. doi:10.1016/j.bone.2010.11.007
21. Carballido-Gamio J, Harnish R, Saeed I, et al. Structural patterns of the proximal femur in relation to age and Hip fracture risk in women. *Bone*. 2013;57:290–299. doi:10.1016/j.bone.2013.08.017
22. Singh M, Nagrath AR, Maini PS. Changes in trabecular pattern of the upper end of the femur as an index of osteoporosis. *J Bone Joint Surg Am*. 1970;52:457–467.
23. Kawashima T, Uhthoff HK. Pattern of bone loss of the proximal femur: a radiologic, densitometric, and histomorphometric study. *J Orthop Res*. 1991;9:634–640. doi:10.1002/jor.1100090503
24. Patel SH, Murphy KP. Fractures of the proximal femur: correlates of radiological evidence of osteoporosis. *Skeletal Radiol*. 2006;35:202–211. doi:10.1007/s00256-005-0065-1
25. Yamamoto N, Sukegawa S, Kitamura A, et al. Deep learning for osteoporosis classification using hip radiographs and patient clinical covariates. *Biomolecules*. 2020;10:1534. doi:10.3390/biom10111534
26. Pramudito JT, Soegijoko S, Mengko TR, Muchtadi FI, Wachjudi RG. Trabecular pattern analysis of proximal femur radiographs for osteoporosis detection. *J Biomed Pharm Eng*. 2007;1:45–51.
27. Link TM, Vieth V, Langenberg R, et al. Structure analysis of high resolution magnetic resonance imaging of the proximal femur: in vitro correlation with biomechanical strength and BMD. *Calcif Tissue Int*. 2003;72:156–165. doi:10.1007/s00223-001-2132-5
28. Sollmann N, Löffler MT, Kronthaler S, et al. MRI-based quantitative osteoporosis imaging at the spine and femur. *J Magn Reson Imaging*. 2021;54:12–35. doi:10.1002/jmri.27260
29. Bonnaire F, Zenker H, Lill C, Weber AT, Linke B. Treatment strategies for proximal femur fractures in osteoporotic patients. *Osteoporos Int*. 2005;16(Suppl 2):S93–S102. doi:10.1007/s00198-004-1746-7
30. Fan J, Lv Y, Xu X, et al. Evaluation of femoral head bone quality by Hounsfield units: a predictor of implant failure for intertrochanteric fractures after intramedullary nail fixation. *Front Surg*. 2022;9:816742. doi:10.3389/fsurg.2022.816742
31. Lee H, Kim SA, Jo S, Jo S. Biomechanical analysis analyzing association between bone mineral density and lag screw migration. *Sci Rep*. 2023;13:747. doi:10.1038/s41598-023-27860-5
32. Kerr R, Resnick D, Sartoris DJ, et al. Computerized tomography of proximal femoral trabecular patterns. *J Orthop Res*. 1986;4:45–56. doi:10.1002/jor.1100040106

33. Stiehl JB, Jacobson D, Carrera G. Morphological analysis of the proximal femur using quantitative computed tomography. *Int Orthop*. 2007;31:287–292. doi:10.1007/s00264-006-0182-z
34. Hambli R, Allaoui S. A robust 3D Finite element simulation of human proximal femur progressive fracture under stance load with experimental validation. *Ann Biomed Eng*. 2013;41:2515–2527. doi:10.1007/s10439-013-0864-9
35. Zhang Y, Zhong W, Zhu H, Chen Y, Xu L, Zhu J. Establishing the 3-D finite element solid model of femurs in partial by volume rendering. *Int J Surg*. 2013;11:930–934. doi:10.1016/j.ijsu.2013.06.843
36. Heimkes B, Posel P, Plitz W, Jansson V. Forces acting on the juvenile Hip joint in the one-legged stance. *J Pediatr Orthop*. 1993;13:431–436. doi:10.1097/01241398-199307000-00003
37. Skuban TP, Vogel T, Baur-Melnyk A, Jansson V, Heimkes B. Function-orientated structural analysis of the proximal human femur. *Cells Tissues Organs*. 2009;190:247–255. doi:10.1159/000210065
38. Reznikov N, Chase H, Ben Zvi Y, et al. Inter-trabecular angle: a parameter of trabecular bone architecture in the human proximal femur that reveals underlying topological motifs. *Acta Biomater*. 2016;44:65–72. doi:10.1016/j.actbio.2016.08.040
39. Tsubota K, Adachi T, Tomita Y. Functional adaptation of cancellous bone in human proximal femur predicted by trabecular surface remodeling simulation toward uniform stress state. *J Biomech*. 2002;35:1541–1551. doi:10.1016/s0021-9290(02)00173-2
40. Tsubota K, Suzuki Y, Yamada T, Hojo M, Makinouchi A, Adachi T. Computer simulation of trabecular remodeling in human proximal femur using large-scale voxel FE models: approach to understanding Wolff's law. *J Biomech*. 2009;42:1088–1094. doi:10.1016/j.jbiomech.2009.02.030
41. Kim J, Chun BJ, Kim JJ. Quantitative load dependency analysis of local trabecular bone microstructure to understand the spatial characteristics in the synthetic proximal femur. *Biology*. 2023;12:170. doi:10.3390/biology12020170
42. Miller Z, Fuchs MB, Arcan M. Trabecular bone adaptation with an orthotropic material model. *J Biomech*. 2002;35:247–256. doi:10.1016/S0021-9290(01)00192-0
43. Boyle C, Kim IY. Three-dimensional micro-level computational study of Wolff's law via trabecular bone remodeling in the human proximal femur using design space topology optimization. *J Biomech*. 2011;44:935–942. doi:10.1016/j.jbiomech.2010.11.029
44. Jang IG, Kim IY. Computational simulation of simultaneous cortical and trabecular bone change in human proximal femur during bone remodeling. *J Biomech*. 2010;43:294–301. doi:10.1016/j.jbiomech.2009.08.012
45. Jang IG, Kim IY. Computational study of Wolff's law with trabecular architecture in the human proximal femur using topology optimization. *J Biomech*. 2008;41:2353–2361. doi:10.1016/j.jbiomech.2008.05.037
46. Schindelin J, Arganda-Carreras I, Frise E, et al. Fiji - an Open Source platform for biological image analysis. *Nat Methods*. 2012;9. doi:10.1038/nmeth.2019
47. Bogovic JA, Hanslovsky P, Wong A, Saalfeld S. Robust registration of calcium images by learned contrast synthesis. 2016 IEEE 13th Int. Symp. Biomed. Imaging ISBI. 2016:1123–1126. doi:10.1109/ISBI.2016.7493463
48. Ward FO. *Outlines of Human Osteology*. Forgotten Books; 2018.
49. Whitehouse WJ, Dyson ED. Scanning electron microscope studies of trabecular bone in the proximal end of the human femur. *J Anat*. 1974;118:417–444.
50. Lu Y, Wang L, Hao Y, Wang Z, Wang M, Ge S. Analysis of trabecular distribution of the proximal femur in patients with fragility fractures. *BMC Musculoskelet Disord*. 2013;14:130. doi:10.1186/1471-2474-14-130
51. Bauer JS, Kohlmann S, Eckstein F, Mueller D, Lochmüller E-M, Link TM. Structural analysis of trabecular bone of the proximal femur using multislice computed tomography: a comparison with dual X-ray absorptiometry for predicting biomechanical strength in vitro. *Calcif Tissue Int*. 2006;78:78–89. doi:10.1007/s00223-005-0070-3
52. Chang G, Honig S, Brown R, et al. Finite element analysis applied to 3-T MR imaging of proximal femur microarchitecture: lower bone strength in patients with fragility fractures compared with control subjects. *Radiology*. 2014;272:464–474. doi:10.1148/radiol.14131926
53. Nazarian A, Muller J, Zurakowski D, Müller R, Snyder BD. Densitometric, morphometric and mechanical distributions in the human proximal femur. *J Biomech*. 2007;40:2573–2579. doi:10.1016/j.jbiomech.2006.11.022
54. Treece GM, Gee AH. Independent measurement of femoral cortical thickness and cortical bone density using clinical CT. *Med Image Anal*. 2015;20:249–264. doi:10.1016/j.media.2014.11.012
55. Treece G, Gee A. Cortical bone mapping: measurement and statistical analysis of localised skeletal changes. *Curr Osteoporos Rep*. 2018;16:617–625. doi:10.1007/s11914-018-0475-3
56. Hall MC. The trabecular patterns of the neck of the femur with particular reference to changes in osteoporosis. *Can Med Assoc J*. 1961;85:1141–1144.